



Spontaneous reduction of O₂ on PtVFe nanocatalysts

Lichang Wang^{a,*}, Joseph I. Williams^a, Tao Lin^{a,b}, Chuan-Jian Zhong^c

^a Department of Chemistry and Biochemistry, Southern Illinois University Carbondale, 1245 Lincon Drive, Carbondale, IL 62901, USA

^b China Tianchen Engineering Corporation, Tianjin 300400, China

^c Department of Chemistry, State University of New York at Binghamton, Binghamton, NY 13902, USA

ARTICLE INFO

Article history:

Received 5 October 2010

Received in revised form 6 January 2011

Accepted 9 January 2011

Available online 9 February 2011

Keywords:

PtVFe ternary nanoparticle

Oxygen reduction reaction

Density functional theory

Molecular adsorption

Dissociative adsorption

Dissociation pathway

ABSTRACT

Reduction of O₂ in the presence of model PtVFe nanocatalysts was studied using the PBE functional with a plane wave basis set. The model catalysts consisted of trimers and a 0.6-nm particle. The results show that among three molecular chemisorption configurations, i.e. Pauling, Griffith, and Yeager configurations, the O₂ bond is weakened the most in the Yeager configuration, then the Griffith configuration, and then the Pauling configuration. A new molecular chemisorption configuration, i.e. 5-atom ring configuration, was also identified. With the O–O distance up to 1.4 Å, a linear correlation was found between the O₂ stretching frequency and the O₂ bond distance regardless of the metal or adsorption site. However, the charge transfer and the adsorption energy are highly dependent on the metal and adsorption site. The alloyed clusters are most effective in transferring electrons to O₂ species and weakening O₂ bond especially when the O atoms are attached to non-Pt atoms. Our results suggest that the superior catalytic activity of PtVFe nanoparticles in the oxygen reduction is due to the effectiveness in charge transfer and the presence of direct (spontaneous) dissociation pathway.

© 2011 Elsevier B.V. All rights reserved.

1. Introduction

One of the most significant challenges for proton exchange membrane (PEM) cell applications is the kinetic limitation of oxygen reduction reaction (ORR) at the cathode at temperatures lower than 100 °C. The traditional catalyst used in the cathode of a PEM cell is platinum. Studies of O₂ reduction on a single Pt atom, clusters, or surfaces have been carried out extensively [1–18]. Great efforts have been made towards developing active, robust, and low-cost electrocatalysts for ORR including Pt-containing multi-metallic nanoparticles [19–98]. For instance, the ternary PtVFe catalysts, prepared by pre-synthesized trimetallic nanoparticles, have been shown to exhibit superior electrocatalytic activities for ORR in actual fuel cells [97,98]. Although many exciting reports can be found on the improved performance of catalysts on ORR, the reaction mechanism is still not well understood, partially due to the complex reaction pathways exhibited by ORR [99–103]. For instance, most recently, Goddard's group has studied the solvent effect on the ORR and their results suggested that alternative mechanisms must be considered other than the well-known plausible 4-electron or 2-electron mechanisms [101].

Reaction pathways for ORR in the presence of multi-component nanoparticles are even more complicated than the single-element nanoparticles. The recent experimental work by Li et al. suggests

that the ORR catalyzed by Co-N/C catalysts is a mixture of 2- and 4-electron transfer pathways, dominated by a 4-electron transfer process [104]. Furthermore, as the results have demonstrated in Goddard's group, the preferable reaction pathways could be altered when solvent is considered [101]. On the other hand, the central theme of the ORR is ultimately the breaking of O–O bond, either in a pure O₂ or an O–OH environment. We, therefore, chose to study breaking O–O bond of O₂ as a representative reaction for the ORR. Moreover, we chose to use trimers and a 0.6-nm particle as the model nanocatalysts in the density functional theory (DFT) study.

Molecular chemisorption of O₂ molecules on Pt catalysts can take place in three distinguished configurations. The first adsorption configuration is denoted as the Pauling model where only one O atom in O₂ is bonded to a metal atom. The second configuration is denoted as the Griffith model where both O atoms are bonded to a single metal atom. The third configuration is denoted as Yeager model where two O atoms are bonded to two metal atoms. In Fig. 1, these three molecular adsorption configurations are illustrated using a Pt₃ trimer as an example. Among the three molecular chemisorption configurations, the Pauling and Yeager configurations have been studied more extensively theoretically. Two states denoted as superoxo-like (O₂^{−δ}) and peroxo-like (O₂^{−2δ}) species have been identified [3]. It has been proposed that peroxo-like states are associated with the Yeager configuration and the superoxo-like states to the Pauling configuration [3]. The stretching frequency and bond length of the adsorbed O₂ are also associated closely with the adsorption configurations. For instance, in the study of O₂ adsorption to one Pt atom in the presence of

* Corresponding author. Tel.: +1 618 453 6476; fax: +1 618 453 6408.
E-mail address: lwang@chem.siu.edu (L. Wang).

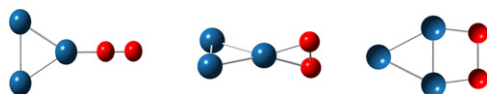


Fig. 1. Three molecular chemisorption configurations of an O₂ to a metal cluster: the Pauling model (left), the Griffith model (middle), and the Yeager model (right). Red and blue balls represent O and Pt atoms, respectively. (For interpretation of the references to color in this figure legend, the reader is referred to the web version of the article.)

organic molecules, Cramer et al. have shown that the superoxo-like species have a bond length of about 1.2–1.3 Å while the peroxo-like species have a bond length of 1.4–1.5 Å [8]. The reported frequency range associated with two different adsorption states, however, are different. Cramer et al. found the adsorbed O₂ frequencies are 1050–1200 cm^{−1} and 800–980 cm^{−1} for the superoxo-like and peroxo-like species, respectively. Siegbahn and Panas calculations gave the frequency range of 870–1020 cm^{−1} for the superoxo-like species and 610–660 cm^{−1} for the peroxo-like species [7]. Even earlier studies by Vaska gave the frequency range of 1075–1195 cm^{−1} for the superoxo-like species and 790–932 cm^{−1} for the peroxo-like species.

Dissociative chemisorption of O₂ molecules in the presence of Pt catalysts has been studied as well [6,15,16,105–110]. It was believed the O₂ dissociation takes place mostly through a barrier and the activation energy from the peroxo-like precursor is about 0.29 eV [15]. Nolan et al. has shown that direct (spontaneous) pathways for O₂ dissociation on Pt surfaces are negligible [15]. The dissociation mechanism may be changed by altering the dissociation energy barrier or by stabilizing the precursor and transition states [106] as well as the chemisorbed species in the vicinity of the O₂ that is to be dissociated [16].

Platinum has traditionally been the metal of choice, but other alternatives are being explored due partly to the high cost and modest activity of platinum with respect to the ORR. Since the late 90s, bimetallic nanoparticles, such as PtAu, [111] PtNi, [10,112,113] PtCo, [10,112–114] PtCr, [113] PtMn, and PtFe, [114] have been found not only to provide some further flexibility of tuning catalytic activities in oxygen reduction reactions but also to have substantially higher activity. In the study of reaction barriers, Anderson et al. have found that the reaction barriers are not very different in the presence of pure Pt with respect to PtNi or PtCo alloys [10]. Using the transition state theory, they further attributed the fast O₂ reduction reaction using the bimetallic alloys to the large prefactor.

Ternary Pt_mV_nFe_k nanoparticles have been shown experimentally to exhibit superior catalytic activities for O₂ reduction over the pure Pt or bimetallic PtNi and PtFe nanoparticles [96–98]. The Pt_mV_nFe_k nanoparticles were found to be four times as active as the commercially available Pt catalysts and two times as active as the PtFe nanoparticles. Except for the high catalytic activities of the ternary Pt_mV_nFe_k catalysts, no other characterizations of detailed mechanistic aspects, such as the adsorption site, the electronic state of the adsorbed O₂ species, and the O₂ stretching frequency, were available. To better understand the reaction mechanism of the ternary Pt_mV_nFe_k nanoparticle and to provide further insight into searching for more active and sustainable O₂ reduction reaction catalysts, it is critical to investigate the ternary Pt_mV_nFe_k nanoparticles both experimentally and theoretically.

Therefore, we chose to study the O₂ molecular and dissociative adsorptions on a model Pt_mV_nFe_k catalyst and report here the first results obtained for these systems. In this work, the PtVFe trimer and a 0.6-nm PtVFe particle were chosen as the model catalysts. For comparison purposes, the catalytic activities of Pt₃ trimer and PtFe₂ trimer on the O₂ adsorption were also studied. To select model catalysts, we also studied bare metal dimers and trimers with all possible compositions. Density functional theory calculations were

performed on these model systems. Detailed description of the computational techniques is given in Section 2. The O₂ molecular adsorption was investigated with all three adsorption configurations, i.e. the Pauling, the Griffith, and the Yeager model. Adsorption energy, charge transfer to the O atoms, and the O₂ stretching frequency were obtained from the DFT calculations. These results are given in Section 3 together with discussion and comparisons with other pure Pt or bimetallic PtFe systems. Finally, the conclusion is drawn in Section 4.

2. Computational details

The calculations were carried out using spin-polarized DFT method that is implemented in Vienna Ab-initio Simulation Package (VASP) [115–117]. The electron–ion interactions were described by Projector Augmented Waves (PAW) method [118]. The exchange and correlation energies were calculated using the Perdew–Burke–Ernzerhof (PBE) functional [119]. A plane wave basis set was used with a cutoff energy of 400 eV. Only the Γ point is needed for finite systems and therefore was used in this work. Furthermore, the size of the unit cell was chosen such that the nearest distance between neighboring images was more than 10 Å. All the parameters, such as the cutoff energy and the size of unit cell, were tested for the convergence of results. The above computational techniques had been used in our previous studies of transition metal clusters, e.g., in the studies of Pt_n, [120] Au_n, [121] Mo_n, [122] CO adsorption on PtAu clusters, [123] and dehydrogenation of CH₄ in the presence of Pt clusters [124].

We studied more than 40 bare binary and ternary PtVFe dimers and trimers in order to understand the structures of these binary and ternary clusters and to obtain the most stable model catalyst structures of PtVFe, PtFe₂, and Pt₃. In order to simulate the catalysts close to those used in the experiments, we also studied 9 isomers of ~0.6 nm consisting of 13 atoms–4 Pt atoms, 2 V atoms, and 7 Fe atoms. This particular composition was chosen for it is within the experimental range. Using the most stable structures as the model catalysts, we investigated both O₂ molecular and dissociative chemisorptions. Specifically, we studied the interactions between the metal clusters and the O₂ molecule for 22 O₂–PtVFe complexes. Three types of calculations were performed for each system, namely structural relaxation calculation, frequency calculation, and Bader charge density analysis [125]. In most cases, we performed calculations without spin restriction. In some cases, we performed spin-restricted calculations in order to confirm that the results from the spin unrestricted calculations are indeed the lowest electronic states or to obtain information on different electronic states. In all geometry optimization calculations, no constraints were applied except for the cases mentioned explicitly in Section 3.3. From these calculations, we obtained the total energy of the system, spin multiplicity, the energy gap between the highest occupied molecular orbital and the lowest unoccupied molecular orbital (HOMO–LUMO energy gap), frequencies, and charge distributions. Based on the total energy of the system, we also calculated binding energy and adsorption energy, which is defined as follows.

For a bare Pt_mV_nFe_k cluster consisting of *m* Pt atoms, *n* V atoms, and *k* Fe atoms, its binding energy is calculated using

$$E_b = -\frac{E_{\text{PtVFe}} - m \times E_{\text{Pt}} - n \times E_{\text{V}} - k \times E_{\text{Fe}}}{m + n + k}, \quad (1)$$

where *E*_{PtVFe}, *E*_{Pt}, *E*_V, and *E*_{Fe} are the total energy of the cluster Pt_mV_nFe_k (*m* = 0–4, *n* = 0–3, and *k* = 0–3, 7), the energy of an isolated Pt atom, the energy of an isolated V atom, and the energy of an isolated Fe atom, respectively. A positive binding energy indicates a stable structure compared to their asymptotic states. As shown in Eq. (1), the calculated binding energies can be used to compare the relative stability between two clusters.

The O₂ adsorption energy is defined to measure the strength of O₂ adsorption to the Pt_mV_nFe_k cluster and is calculated as:

$$E_{\text{Ads}} = -(E_{\text{O}_2-\text{Pt}_m\text{V}_n\text{Fe}_k} - E_{\text{Pt}_m\text{V}_n\text{Fe}_k} - E_{\text{O}_2}), \quad (2)$$

where $E_{\text{O}_2-\text{Pt}_m\text{V}_n\text{Fe}_k}$, $E_{\text{Pt}_m\text{V}_n\text{Fe}_k}$, and E_{O_2} are the total energy of the O₂-Pt_mV_nFe_k complex, the isolated Pt_mV_nFe_k cluster ($m = 1, 3, 4$, $n = 0-2$, and $k = 0-2, 7$), and the isolated O₂ molecule, respectively. The Bader charge transfer to O₂ species, $\Delta e_{\text{O}_2^-}$, is calculated by:

$$\Delta e_{\text{O}_2^-} = e^-(\text{O}_2-\text{Pt}_m\text{V}_n\text{Fe}_k) - 12, \quad (3)$$

where $e^-(\text{O}_2-\text{Pt}_m\text{V}_n\text{Fe}_k)$ represents the number of valence electrons attached to the O₂ species in the adsorbed O₂-Pt_mV_nFe_k complex and 12 represent the valence electrons of a O₂ species in gas phase.

3. Results and discussion

In order to study O₂ chemisorptions on model ternary Pt_mV_nFe_k catalysts, we studied the dimers and trimers with all possible compositions so that the most stable bare clusters can be used in adsorption calculations. In the first part of this section, we present the DFT results in bare cluster studies followed by presentations of the results on the O₂ molecular and dissociative adsorption, respectively. We will also present the results on the O₂ adsorption on a PtVFe particle of 0.6 nm to verify the conclusions drawn from the studies based on trimers.

3.1. Bare metal clusters

Six dimers and thirty-four trimers were studied with respect to binding energy, HOMO–LUMO energy gap, and cluster geometry. Six possible configurations of dimers were studied with three X₂ and three XY configuration: X₂ = Pt₂, V₂, Fe₂ and XY = PtV, PtFe, VFe. All six bimetallic compositions of trimers were studied: Pt₂V, PtV₂, Pt₂Fe, PtFe₂, V₂Fe and VFe₂. Linear bimetallic trimers with a composition of X₂Y can be arranged in two distinct configurations XXY or XYX. Furthermore, single element clusters Pt₃, Fe₃ and V₃, as well as the smallest trimetallic alloy PtVFe were studied. The results for the linear and triangular structures are shown in Tables 1 and 2, respectively.

Among the six dimers shown in Table 1, the stability is in the order of PtV > PtFe > Pt₂ > V₂ > VFe > Fe₂. However, there are no apparent correlation between the stability and the other quantities, such as spin state or HOMO–LUMO gap. For linear trimers shown in Table 1, the relative stability is Pt₂V > PtVFe > Pt₂Fe > PtV₂ > Pt₃ > PtFe₂ > V₂Fe > VFe₂ > V₃ > Fe₃. Examining the linear structures of PtVFe (the last three structures in Table 1), we see that the structure is most stable when V is at the center. The second most stable structure places Fe at the center, and the least stable structure is VPtFe. This is somehow surprising at first if we make predictions based on the binding energy of bimetallic dimers. Based on the data of bimetallic dimers in Table 1, we would expect the stability of PtVFe linear trimers decreases from VPtFe to PtVFe to PtFeV. However, if we take the spin into consideration of binding in trimers as well, the current result seems understandable. Among the bimetallic pairs, V has the ability of lowering the spin state. This trend, i.e. V prefers to be in the middle then iron then Pt, holds in the bimetallic trimers as well. Each bimetallic trimer has two configurations, depending on the identity of the center atom. Results in Table 1 show that for every bimetallic trimer that contains vanadium, the most stable structure is with vanadium at the center. Similarly, for every bimetallic trimer consisting of iron, the most stable configuration is with iron in the middle when the other metal is platinum, otherwise the vanadium is in the middle. The only exception to this trend is V₂Fe, where the most stable configuration is VFeV.

Table 1

Binding energy, E_b (eV/atom), bond distances, r (Å), spin multiplicity ($2S+1$), and HOMO–LUMO energy gap, $\Delta E_{\text{H-L}}$ (eV), of bare metal dimers and linear trimers.

	E_b	r	$2S+1$	$\Delta E_{\text{H-L}}$
Pt ₂	1.88	2.33	3	0.86
V ₂	1.82	1.72	3	1.34
Fe ₂	1.28	1.98	7	0.24
PtV	2.33	2.12	4	0.43
PtFe	2.00	2.17	5	0.01
VFe	1.70	1.74	2	0.10
Pt ₃	2.25	2.36 (2) ^a	5	2.25
V ₃	1.52	1.72 (2)	8	0.35
Fe ₃	0.83	1.87 (2)	5	0.22
PtVPt	3.14	2.11 (2)	2	0.44
PtPtV	2.38	2.39, 2.09 ^b	2	0.01
PtFePt	2.44	2.24 (2)	7	2.76
PtPtFe	2.18	2.41, 2.19	7	0.29
PtPtFe	2.15	2.40, 2.18	5	1.73
VVPt	2.42	1.64, 2.19	3	0.56
VPtV	2.18	2.27 (2)	9	0.01
VPtV	2.08	2.27 (2)	7	0.20
VPtV	1.82	2.27, 2.39	1	0.10
FeFePt	1.98	2.30, 2.19	9	0.72
FePtFe	1.95	2.27 (2)	9	1.50
VFeV	1.78	2.00 (2)	7	0.86
VVFe	1.70	2.25, 1.75	7	1.26
VVFe	1.64	1.59, 2.37	3	0.16
FeVFe	1.68	1.92 (2)	4	0.77
FeFeV	1.55	2.31, 1.67	4	0.31
PtVFe	2.52	2.15, 1.67	2	1.18
PtFeV	2.30	2.19, 1.70	2	0.75
VPtFe	1.79	2.16, 2.34	2	0.07

^a (2) denotes two of the same bond distance.

^b 2.39 is Pt–Pt distance and 2.09 is Pt–V distance.

The results for triangular trimers are provided in Table 2. The binding energy decreases from top trimer Pt₂V to the bottom trimer, Fe₃. Comparing the linear and the corresponding triangular trimers, data in Tables 1 and 2 show that in all but one case, Pt₂V, the triangular clusters are more stable than the corresponding linear isomers. We would also like to point out that many nearly degenerate electronic states exist in the multi-metallic systems. In Table 1, we showed two nearly equally stable structures VVFe with different spin states. Two different electronic states for the PtPtFe cluster were also found to be energetically degenerate. These closely lying states may all play important roles in the O₂ reduction reaction.

The structure and relative energy of nine Pt₄V₂Fe₇ isomers are presented in Fig. 5. The initial structures of these isomers have the same bulk-like fcc structure but differ in homogeneity. As shown in Fig. 5, the relaxed structures are completely different from the initial fcc structures except for structure 8. The most stable isomer was found to be structure 3 and used in the subsequent adsorption calculations.


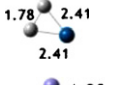
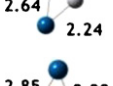
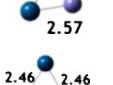
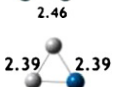
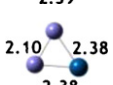
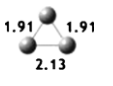
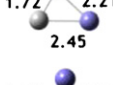
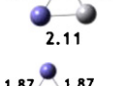
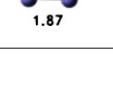
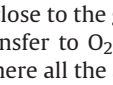
3.2. O₂ molecular chemisorptions

Various molecular adsorption complexes were investigated in order to understand O₂ molecular chemisorption on PtVFe, Pt₃, and PtFe₂ clusters. Many different initial orientations of O₂ with respect to the trimer were studied and the adsorption complexes were relaxed to the three adsorption configurations shown in Fig. 1, i.e. Pauling, Griffith, and Yeager model, but one structure shown in Table 3 as complex 15. DFT results of sixteen adsorption complexes are presented in Table 3. In the following, we discuss the O₂ adsorption on Pt₃ then on PtFe₂ then on PtVFe.

The O₂–Pt₃ adsorption complexes are illustrated as structures 1–4 in Table 3. These results reveal several trends in relation to the adsorption configuration of the M–O bonds. Pauling configuration gives smaller adsorption energy and consequently has a higher O₂ vibrational frequency. The O₂ bond distance in a Pauling configu-

Table 2

Structure, binding energy, E_b (eV/atom), bond distances (Å), spin multiplicity ($2S + 1$), and HOMO–LUMO energy gap, ΔE_{H-L} (eV), of bare triangular trimers. Blue, gray, and purple balls represent Pt, V, and Fe atoms, respectively.

	Structure	E_b	$2S + 1$	ΔE_{H-L}
Pt ₂ V		2.89	2	0.41
PtV ₂		2.75	3	0.66
PtVFe		2.63	1	0.77
Pt ₂ Fe		2.50	4	0.71
Pt ₃		2.41	1	0.09
PtV ₂		2.34	6	0.17
PtFe ₂		2.31	8	0.48
V ₃		2.05	7	0.35
V ₃ Fe		2.01	4	0.54
VFe ₂		1.83	5	1.21
Fe ₃		1.72	4	0.22

ration is very close to the gas phase value of 1.241 Å. Furthermore, the charge transfer to O₂ is less effective. The exception here is structure 1, where all the atoms are in the same plane. This planar arrangement may facilitate charge transfer more efficiently. The Griffith and Yeager configurations, on the other hand, show a better charge transfer with substantially smaller O₂ stretching frequency and longer O₂ bond length.

The results of calculated O₂–PtFe₂ adsorption complexes are shown in Table 3 as structures 5–8. It is apparent that the properties of these complexes are highly dependent upon the metal to which the O₂ binds. When the O₂ binds to Pt site, the same trends as the O₂–Pt₃ complexes can be identified. For instance, the less stable Pauling structure 5 has a higher O₂ vibrational frequency, less amount of charge transfer, and shorter O₂ bond distance than the Griffith structure 7. In terms of adsorption at the Fe site versus Pt site, O₂ binds more strongly to the Fe site. The adsorption complex with Fe involved in binding has a lower O₂ vibrational frequency, longer O₂ bond length, and larger charge transfer. These findings are true for both the Pauling configuration (structures 5 and 6) as well as the Griffith configuration (structures 7 and 8). It is worth mentioning that no stable Yeager structures were identified for O₂–PtFe₂ complexes, as all the initial starting geometries resembled the Yeager configuration yielded O₂ dissociation.

Comparing the O₂–Pt₃ and the O₂–PtFe₂ adsorption complexes, results show that O₂ adsorption strength decreases from PtFe₂ to Pt₃ if the adsorption is to the Pt site. However, the O–O distance and charge transfer increase and the O₂ stretching frequency decreases. This indicates that alloying is beneficial in weakening the O–O bond at the same time making the adsorbates less strongly attached to the catalytic sites.

Results on eight O₂–PtVFe complexes are provided in Table 3. Similar to the O₂–PtFe₂ complexes, the O₂ adsorptions on PtVFe clusters are highly dependent upon the metal site to which O₂ is adsorbed and the adsorption configuration. Within the Pauling configuration, structures 9–12 in Table 3, the complex with the O₂ bound to vanadium site is the most energetically favorable structure. It is also the most effective in charge transfer. However, it is not necessarily the most effective at lengthening the O₂ bond or decreasing the O₂ stretching frequency. In particular, structures 11 and 12 are more stable than structures 9 and 10, but have a much higher O₂ frequency and shorter O₂ bond length. No stable structures of O₂ bound to Fe in the Pauling configuration were identified, as all initial structures were relaxed to structure 10 in Table 3.

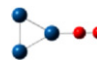
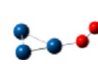
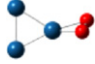
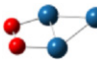








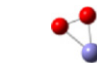

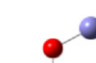

Within the Griffith configuration, shown as structures 13 and 14 in Table 3, the complex with the O₂ attached to the V site is energetically favorable and has either equivalent or more effective characteristics than that to the Fe site. No stable structures of O₂ bound to the Pt site were found in the Griffith structure, as all initial configurations were relaxed to structure 10 in Table 3. A 5-atom ring structure, structure 15, was obtained. Although its adsorption energy is similar to those of structures 9 and 10, it is the most efficient PtVFe complex towards weakening O₂ bond, i.e. longer bond distance and lower frequency.

The comparison of results on the O₂ adsorption on different clusters, PtVFe, PtFe₂, and Pt₃, shows alloying favors stretching O–O bond when the adsorption site is Pt, though the adsorption energy decreases. In the Pauling configuration, structures 5, 9, and 10 in Table 3 have lower O₂ vibrational frequencies, longer O₂ bond lengths, and larger charge transfers than structure 2. In the study of O₂ dissociation in the presence of various metals, Cramer et al. found an inverse relationship between frequency and bond length (see the yellow line with diamonds in Fig. 2(a)) [8] (for interpretation of the references to color in this text, the reader is referred to the web version of the article). Plotting this relationship utilizing our data yielded a similar relationship, in particular, when the O₂ bond length was smaller than 1.4 Å, which corresponds to the Pauling structures (circles in Fig. 2(a)). There was a broadening of the data around the correlation line when the O–O bond length is greater than 1.4 Å. Using different adsorption configurations, we can explain this broadening.

Given the fact that the bond distances above the 1.4-Å range correspond mainly to the Griffith and Yeager configurations, it is feasible that multiple correlations exist depending on the adsorption configuration. Under this model, the O₂ bond lengths in Pauling configuration would be most sensitive to the O₂ vibrational frequency. Griffith configuration would appear to maintain a consistent O₂ vibrational frequency over a wide range of bond lengths after the bond length stretches beyond 1.4 Å (see the red line with triangles of Fig. 2(a)). Yeager structures would maintain a consistent bond length over a wide range of vibrational frequencies (green line with squares in Fig. 2(a)). The lack of strong interaction between the oxygen atoms when the bond length is greater than 1.4 Å can be understood by the fact that the O₂ molecule is close to the dissociation threshold.

Interestingly, the amount of charge transfer to the O atoms has shown different trends, as depicted in Fig. 2(b). Within the Pauling adsorption mode, there are no apparent trends (demonstrated by the circles in Fig. 2(b)). However, under both Griffith and Yeager modes, the amount of charge transfer increases with the O–O

Table 3
Adsorption energy, E_{Ads} (eV), O_2 stretching frequency, ν_{O_2} (cm^{-1}), electron transfer to the O_2 species, $\Delta e_{\text{O}_2^-}$, O–O distance (\AA), spin multiplicity, $2S+1$, and HOMO–LUMO energy gap, $\Delta E_{\text{H-L}}$ (eV), of molecularly adsorbed O_2 systems. Red, blue, gray, and purple balls represent O, Pt, V, and Fe atoms, respectively.

	1	2	3	4	5	6	7	8
								
E_{Ads}	1.71	1.83	1.94	1.79	0.87	1.82	1.20	2.87
ν_{O_2}	1260	1180	1025	764	1185	1171	1047	987
$\Delta e_{\text{O}_2^-}$	0.73	0.50	0.57	0.64	0.51	0.59	0.58	0.87
O–O	1.285	1.296	1.405	1.412	1.303	1.311	1.388	1.448
$2S+1$	1	1	1	3	7	7	9	9
$\Delta E_{\text{H-L}}$	0.18	0.23	0.34	0.57	0.48	0.28	1.14	0.85
	9	10	11	12	13	14	15	16
								
E_{Ads}	1.14	1.17	2.21	2.24	2.52	3.81	1.60	3.69
ν_{O_2}	1102	1052	1203	1192	1006	1008	778	871
$\Delta e_{\text{O}_2^-}$	0.52	0.56	0.90	0.87	0.86	1.12	0.86	1.07
O–O	1.326	1.361	1.320	1.326	1.432	1.471	1.422	1.453
$2S+1$	2	2	4	2	2	2	2	2
$\Delta E_{\text{H-L}}$	0.48	0.72	1.09	0.25	0.37	0.49	0.65	1.01

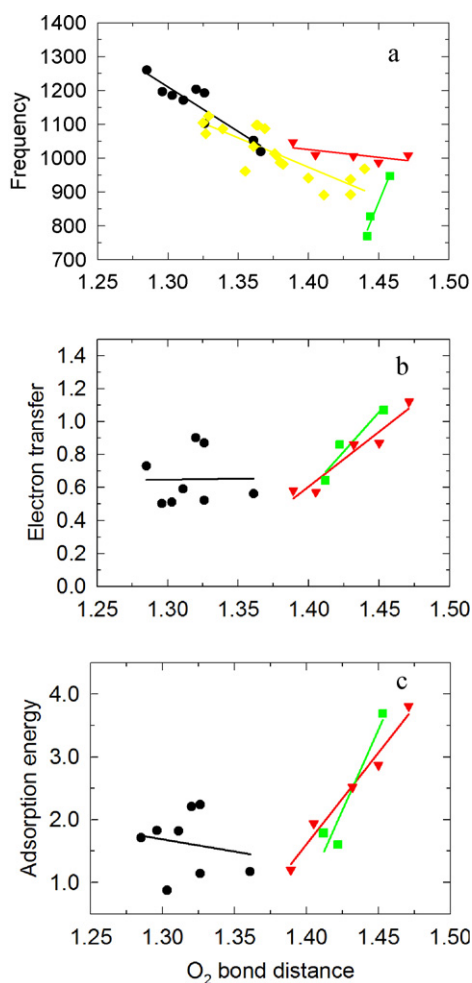


Fig. 2. O_2 frequency (cm^{-1}) (a), the number of electrons transferred to O_2 (b), and the adsorption energy (eV) (c) as a function of O_2 bond distance (\AA) among different metal complexes. The circles, triangles, and squares represent the data obtained from the current calculations for the Pauling, the Griffith, and the Yeager structures, respectively. The diamonds in (a) are the data from Ref. [8].

distance. The same observations can be made on the correlation between the adsorption energy and the O–O distance, shown in Fig. 2(c).

3.3. O_2 dissociative chemisorptions

O_2 dissociative chemisorptions on Pt catalysts have been studied extensively [6,15,16,105–110]. It was established that dioxygen dissociation occurs through a barrier and the activation energy from the peroxo-like precursor is about 0.29 eV [15]. Moreover, direct (spontaneous) pathways for O_2 dissociation on Pt surfaces are negligible [15]. The dissociation mechanism may be changed by altering the dissociation energy barrier or by stabilizing the precursor and transition states, [106] as well as by adjusting the type of chemisorbed species in the vicinity of the adsorbed O_2 [16]. For multi-metallic catalysts, we illustrate here that the mechanism may be affected by the dissociation sites of different compositions. Indeed, the reaction for O_2 approaching the V–Fe site of a PtVFe trimer takes an indirect dissociation pathway, different from the direct dissociation pathway via the Pt–V site.

Five dissociation complexes were obtained from our DFT calculations and these results are shown in Table 4. The results illustrate that PtVFe and PtFe₂ are more effective at transferring charge to atomic O after dissociation. To explore dissociation pathways, we studied two systems starting from O_2 –Pt₃ (structure 4 in Table 3) and from O_2 –PtVFe (structure 16 in Table 3) to the O_2 dissociation. Since the spin multiplicities of the initial and final structures for PtVFe differed, two separate potential energy curves were calculated based upon each multiplicity. These results are shown in Figs. 3 and 4. As shown in Fig. 4, the O_2 dissociation in the presence of PtVFe may involve spin crossing. However, the crossing takes place rather late in the dissociation process, i.e. at very late stage of O–O bond breaking. Therefore, no further investigations were made here on the spin crossing process, such as the exact crossing point along the reaction pathway or whether such a crossing is allowed. Furthermore, the optimization calculations for the data points in Figs. 3 and 4 between the initial and final structures were obtained by fixing the O–O distance at each point but allowing other degrees of freedom to relax.

Table 4

Adsorption energy, E_{Ads} (eV), O–M frequency, $\nu_{\text{O-M}}$ (cm^{-1}), electron transfer to the O_2 species, $\Delta e_{\text{O}_2^-}$, M–O distance (Å), spin multiplicity, $2S+1$, and HOMO–LUMO energy gap, $\Delta E_{\text{H-L}}$ (eV), of dissociative O_2 systems. Red, blue, gray, and purple balls represent O, Pt, V, and Fe atoms, respectively.

	d1	d2	d3	d4	d5
E_{Ads}	3.24	4.50	4.24	4.75	7.69
$\nu_{\text{O-M}}$	861	684	976	817	1037
	843	585	829	769	758
		585		357	479
$\Delta e_{\text{O}_2^-}$	1.29	1.23	1.47	1.87	1.85
M–O	1.76	1.79 (Pt)	1.60	1.73 (V)	1.63 (V)
	1.76	1.80 (Fe)	1.62	1.81 (Pt)	1.78 (V)
		1.80 (Fe)		2.00 (Fe)	1.83 (Fe)
$2S+1$	3	9	7	4	4
$\Delta E_{\text{H-L}}$	0.58	0.26	0.14	1.07	1.32

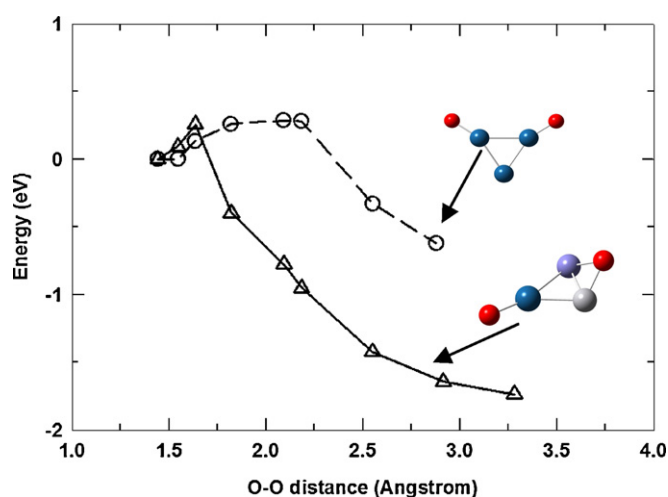


Fig. 3. A comparison of energy profiles for two reaction pathways for O_2 dissociation on PtVFe (solid line with triangles) and Pt_3 (dash line with circles).

The activation energy for the O_2 dissociation on PtVFe, forming the final product shown as structure **d5** in Table 4, is 0.26 eV and that on Pt_3 , forming structure **d1**, is 0.29 eV. The slight difference in activation energy between these model catalysts (~ 0.03 eV) indicates that the ratio of dissociation rates does not depend significantly on temperature.

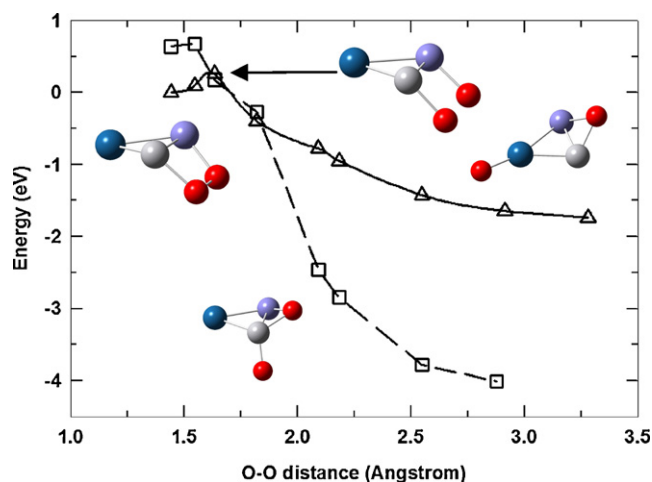


Fig. 4. Two O_2 dissociation pathways on the PtVFe trimer in different spin states: doublet (solid line with triangles) and quintet (dashed line with squares).

The rate constant, k , was calculated using the harmonic transition state theory expressed as, [126,127].

$$k = \frac{\prod v_i}{\prod v_i^\ddagger} e^{-\Delta E/k_B T}, \quad (4)$$

where v_i and v_i^\ddagger are the frequencies of reactant and transition state, respectively. The reaction barrier height, ΔE , is 0.26 eV for the PtVFe trimer and 0.29 eV for the Pt_3 with the reaction pathways depicted in Fig. 3. k_B and T are the Boltzmann constant and temperature, respectively. The frequencies for the transition states were obtained the same way as those for the reactants.

Table 5 shows the rate constant as a function of temperature obtained using Eq. (4) for O_2 dissociation on the model catalysts, PtVFe and Pt_3 trimers. Despite complications involving changes of spin states in the reaction (see Fig. 4), the harmonic transition state theory calculations reveal that O_2 dissociation on the PtVFe trimer, in the indirect dissociation route, is about four times as fast as that on Pt_3 for this particular reaction pathway. The difference in rate constants between the two pathways is due to the combined effect of barrier height and width (reflected by frequencies). We mention that DFT tends to underestimate the barrier height but can generally give a better accuracy in the relative energy. Therefore, we expect that the rate constant ratio should be more reliable than the absolute rate constants.

The DFT calculations presented so far were for O_2 adsorption on metal trimers. On the other hands, our experiments were performed typically on particles of ~ 2 nm. Therefore, the question is whether the conclusions drawn based on trimers can be extended to the observations made experimentally. As the first step to address this issue, we performed calculations for O_2 adsorption on a 0.6-nm PtVFe particle (Fig. 5). The DFT studies of O_2 adsorption on a 13-atom $\text{Pt}_4\text{V}_2\text{Fe}_7$ cluster were carried out. Six of the adsorption complexes are illustrated in Fig. 6. Complex (a) in Fig. 6 is similar structure wise to the complexes **d2** and **d4** in Table 4 but different in bonding atoms. In complex (a), one O atom bonds to V and the other bonds to PtFe. In contrast, in **d2** and **d4**, one O atom

Table 5

The O_2 dissociation rate constant as a function of temperature for the reactions shown in Fig. 3.

T ($^\circ\text{C}$)	k_1 (PtVFe) (s^{-1})	k_2 (Pt_3) (s^{-1})	k_1/k_2
25	4.29×10^9	9.71×10^8	4.4
50	9.39×10^9	2.32×10^9	4.0
75	1.84×10^{10}	4.91×10^9	3.7
100	3.28×10^{10}	9.39×10^9	3.5
125	5.45×10^{10}	1.65×10^{10}	3.3

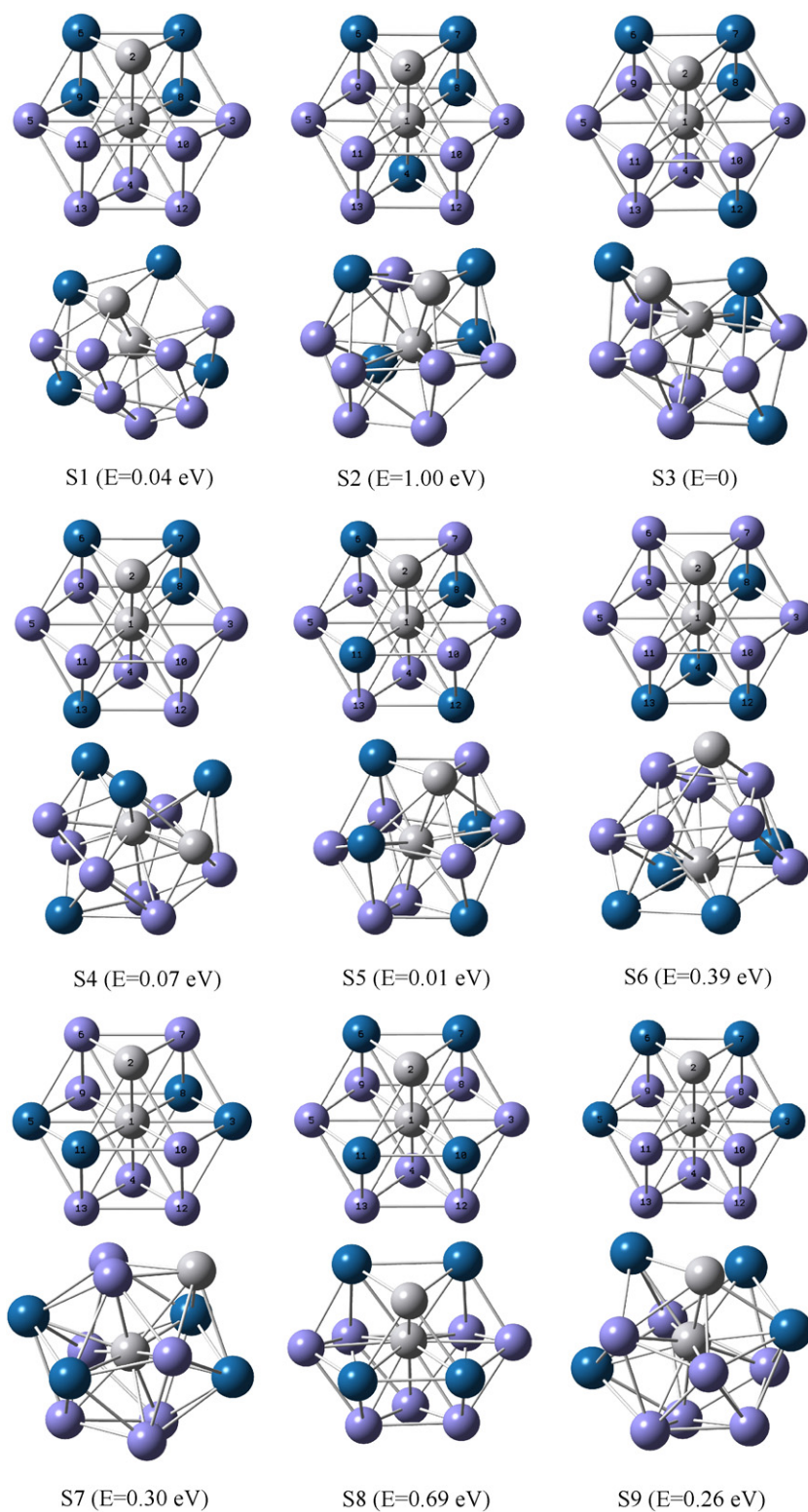


Fig. 5. Initial and final structures of $\text{Pt}_4\text{V}_2\text{Fe}_7$ isomers.

bonds to Pt and the other bonds to FeFe or PtFe, respectively. Complex (b) in Fig. 6 resembles 15 in Table 3. As the O_2 molecule bonds to Fe and Pt in both complexes, the adsorption energies of these complexes are, as expected, similar. Complexes (c) and (f) in Fig. 6 can be compared to 16 in Table 3, though the metal atoms attached to the O atoms are different. Complex (d) in Fig. 6 resembles complexes 9 and 10 in Table 3 in adsorption modes and energy. The

similar adsorption energy between these complexes is due to the same immediate interacting metal atom, Pt, in all cases. Complex (e) in Fig. 6 is compared to d5 in Table 4. The adsorption energies in these complexes are also similar. In summary, despite the differences between the trimer and $\text{Pt}_4\text{V}_2\text{Fe}_7$, there are similarities in the results as described above in the O_2 adsorption and dissociation. Furthermore, the magnitude of the reaction barrier height obtained

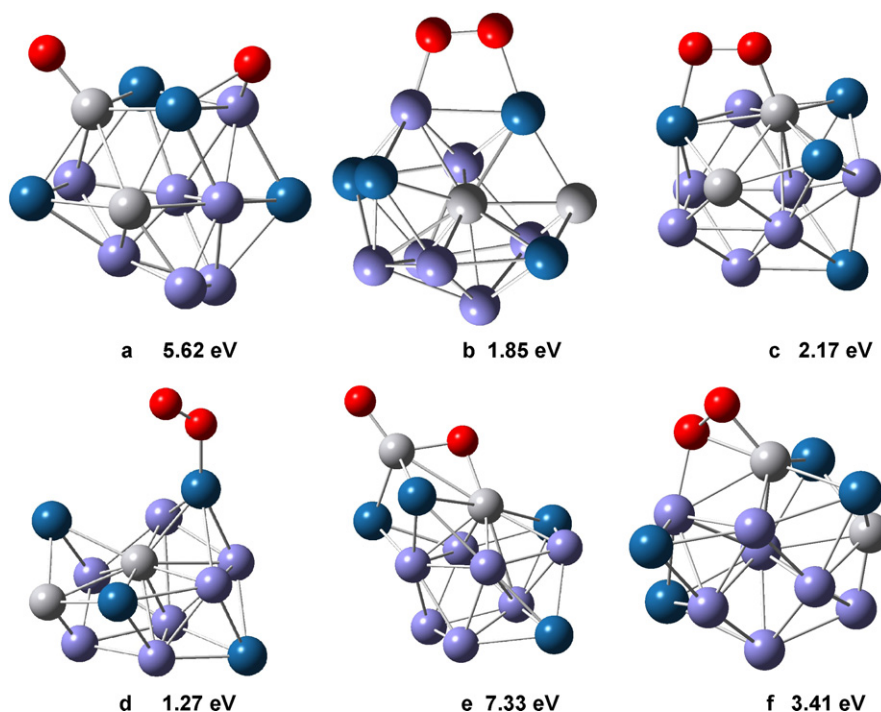


Fig. 6. Structures and adsorption energies of O_2 adsorption on the same bare $Pt_4V_2Fe_7$ cluster (pictured as S3 in Fig. 5) at various adsorption sites.

using Pt3 is essentially the same as that measured on Pt single crystal by Nolan et al. [15] It is also in line with the work of Anderson et al. who found that the activation energies for pure Pt and Pt alloys on unsupported polycrystalline electrodes are similar [10]. These seem to indicate that the trimer model catalysts have captured the essence of the underlying mechanism of O_2 dissociation.

We mention that the calculations of O_2 adsorption on the $PtFe_2$ trimers illustrate that O_2 can also undergo a direct (spontaneous) dissociation. The dissociative structures are shown in Table 4 (d2 and d3). In all cases studied here, the electron transfer to the O species is the largest in $PtVFe$ trimer with respect to $PtFe_2$ or Pt_3 , as shown by the data in Table 4. In addition to the electron transfer, the other contributors that make the $PtVFe$ works better than pure Pt on ORR may include reducing the lattice distance, providing sites for the formation of metal-oxygen bonds and adsorption of OH^- , and changing the d-band center [96]. While the bimetallic $PtFe$ nanoparticles seem to be good catalysts on account of the possibility of direct reaction pathways, the significance of the presence of V element in $PtVFe$ nanoparticles is to enhance the electron transfer, which effectively facilitates the subsequent steps in the ORR process. However, the adsorption energy of 7.69 eV (structure d5 in Table 4) is indicative of a very strong interaction and the formation of oxide species. As such, these active sites are blocked upon the initial adsorption and cannot contribute to the catalytic activities. This analysis reveals that the presence of too much V in the $PtVFe$ nanoparticles results in poisoning of the catalyst. The combination of the significant electron transfer due to the presence of V, the direct pathway at the Pt–V site, and the poisoning owing to the presence of excess V implies that there must be an optimal composition of V.

Furthermore, the catalytic activity for oxygen reduction is determined not only by the ability of a nanoparticle to dissociate O_2 , but also by the subsequent binding of the dissociated products. From the data, it has been shown that a strong oxide product seems to be forming. Formation of oxides would block the active site of the catalyst. However, our experiments have shown that the catalytic activities are consistent. This indicates that the adsorbed atomic

O may subsequently form a different species thus can leave the active site promptly. Further DFT calculations by considering co-adsorption of other species is in progress.

4. Conclusions

DFT studies of O_2 molecular and dissociative chemisorptions on the model ternary $PtVFe$ catalysts, $PtVFe$, Pt_3 , $PtFe_2$, and $Pt_4V_2Fe_7$ were carried out. In order to choose model catalysts and to investigate the homogeneity of surface composition of alloy catalysts, more than 40 bare alloy dimers and trimers with all possible compositions were studied.

Sixteen O_2 – $Pt_mV_nFe_k$ molecular chemisorption complexes were studied with four adsorption configurations. Among the three configurations being studied, Pauling, Griffith, and Yeager model, the O_2 bond is weakened the most in the Yeager configuration, to a less extent in the Griffith configuration, and the least in the Pauling configuration. A 5-atom ring configuration was also found to be stable. A linear correlation can be found among the adsorption complexes between the frequency and the O_2 bond distance up to 1.4 Å. However, within the same O–O distance range, the amount of charge being transferred to the O atoms and the adsorption energy are highly dependent on the metal and adsorption site. The alloyed clusters are most effective in transferring electrons to O_2 species and in weakening O_2 bond.

Based on the study of the five O_2 – $Pt_mV_nFe_k$ dissociative adsorption complexes were studied here: O_2 – $PtVFe$, O_2 – Pt_3 , and O_2 – $PtFe_2$, our results suggest that the catalytic activity of the $Pt_mV_nFe_k$ nanoparticles in the oxygen reduction is mainly due to efficient charge transfer to the oxygen species and spontaneous dissociation pathways.

Finally, we point out that the method developed in this study can be applied to the study of other O_2 –ternary nanoparticle systems. One of such studies under investigation is the O_2 – $PtNiFe$ system, which was demonstrated experimentally to be a promising catalyst for ORR [128]. We also note that the model catalysts chosen in this study are not exactly the same as the catalysts used

in our experiments, where the size of the nanocatalysts was in the range of ~ 1.5 nm and the catalysts were supported by carbon black [96–98]. The similarities shown between the results on trimers and the 0.6-nm particle indicate that the conclusions drawn on the model catalysts are applicable to the catalytic activities exhibited by real catalysts. However, our calculations also show that there are more possible adsorption configurations in the O_2 –Pt $_4$ V $_2$ Fe $_7$ systems than in the O_2 –PtVFe systems. This suggests that further studies on bigger PtVFe nanoparticles are necessary in order to have a complete picture and understanding of our experimental catalysts for the ORR.

Acknowledgement

We acknowledge the National Science Foundation for support of this research under grant CBET-0709113.

References

- [1] T. Jacob, R.P. Muller, W.A. Goddard, *J. Phys. Chem. B* 107 (2003) 9465.
- [2] T. Li, P.B. Balbuena, *J. Phys. Chem. B* 105 (2001) 9943.
- [3] L. Vaska, *Acc. Chem. Res.* 9 (1975) 175.
- [4] X. Lin, N.J. Ramer, A.M. Rappe, K.C. Hass, W.F. Schneider, B.L. Trout, *J. Phys. Chem. B* 105 (2001) 7739.
- [5] E. Yeager, *Electrochim. Acta* 29 (1984) 1527.
- [6] A. Eichler, F. Mittendorfer, J. Hafner, *Phys. Rev. B* 62 (2000) 4744.
- [7] I. Panas, P. Siegbahn, *Chem. Phys. Lett.* 153 (1988) 458.
- [8] C.J. Cramer, W.B. Tolman, K.H. Theopold, A.L. Rheingold, *Proc. Natl. Acad. Sci. U.S.A.* 100 (2003) 3635.
- [9] M.R. Tarasevich, A.J. Sadkowski, E. Yeager, in: B.E. Conway, et al. (Eds.), *Comprehensive Treatise of Electrochemistry*, vol. 7, 1983, p. 301.
- [10] A.B. Anderson, J. Roques, S. Mukerjee, V.S. Murthi, N.M. Markovic, V. Stamenkovic, *J. Phys. Chem. B* 109 (2005) 1198.
- [11] V. Stamenkovic, B.N. Grgur, P.N. Ross, N. M. Markovic 152 (2005) A277.
- [12] C. Puglia, A. Nilsson, B. Hernnas, O. Karis, P. Bennich, N. Martensson, *Surf. Sci.* 342 (1995) 119.
- [13] P.D. Nolan, B.R. Lutz, P.L. Tanaka, J.E. Davis, C.B. Mullins, *Phys. Rev. Lett.* 81 (1998) 3179.
- [14] A. Eichler, J. Hafner, *Phys. Rev. Lett.* 79 (1997) 4481.
- [15] P.D. Nolan, B.R. Lutz, P.L. Tanaka, J.E. Davis, C.B. Mullins, *J. Chem. Phys.* 111 (1999) 3696.
- [16] T. Zambelli, J.V. Barth, J. Winterlin, G. Ertl, *Nature* 390 (1997) 495.
- [17] Q. Ge, P. Hu, D.A. King, M.-H. Lee, J.A. White, M.C. Payne, *J. Chem. Phys.* 106 (1997) 1210.
- [18] A. Gross, A. Eichler, J. Hafner, M.J. Mehl, D.A. Papaconstantopoulos, *Surf. Sci.* 539 (2003) L542.
- [19] Y.H. Bing, H.S. Liu, L. Zhang, D. Ghosh, J.J. Zhang, *Chem. Soc. Rev.* 39 (2010) 2184.
- [20] C.J. Zhong, J. Luo, B. Fang, B.N. Wanjala, P.N. Njoki, R. Loukrakpam, J. Yin, *Nanotechnology* 21 (2010) 062001.
- [21] C.J. Zhong, J. Luo, P.N. Njoki, D. Mott, B. Wanjala, R. Loukrakpam, S. Lim, L. Wang, B. Fang, Z. Xu, *Energy Environ. Sci.* 1 (2008) 454.
- [22] J. Zhang, K. Sasaki, E. Sutter, R.R. Adzic, *Science* 315 (2007) 220.
- [23] T. He, E. Kreidler, L. Xiong, E. Ding, *J. Power Sources* 165 (2007) 87.
- [24] K.C. Neyerlin, W. Gu, J. Jorne, H.A. Gasteiger, *J. Electrochem. Soc.* 153 (2006) A1955.
- [25] V. Mazumder, M.F. Chi, K.L. More, S.H. Sun, *J. Am. Chem. Soc.* 132 (2010) 7848.
- [26] Y.S. Hu, X. Liu, J.O. Muller, R. Schlögl, J. Maier, D.S. Su, *Angew. Chem. Int. Ed.* 48 (2009) 210.
- [27] K. Gong, F. Du, Z. Xia, M. Durstock, L. Dai, *Science* 323 (2010) 760.
- [28] J. Greeley, I.E.L. Stephens, A.S. Bondarenko, T.P. Johansson, H.A. Hansen, T.F. Jaramillo, J. Rossmeisl, I. Chorkendorff, J.K. Nørskov, *Nat. Chem.* 1 (2009) 552.
- [29] B. Lim, M. Jiang, P.H.C. Camargo, E.C. Cho, J. Tao, X. Lu, Y. Zhu, Y. Xia, *Science* 324 (2009) 13021305.
- [30] S.W. Lee, S. Chen, J. Suntivich, K. Sasaki, R.R. Adzic, Y. Shao-Horn, *J. Phys. Chem. Lett.* 1 (2010) 1316.
- [31] M.W. Louie, A. Hightower, S.M. Haile, *ACS Nano* 4 (2010) 2811.
- [32] T. Ikeda, M. Boero, S.F. Huang, K. Terakura, M. Oshima, J. Ozaki, S. Miyata, *J. Phys. Chem. C* 114 (2010) 8933.
- [33] E.J. Biddinger, U.S. Ozkan, *J. Phys. Chem. C* 114 (2010) 15306.
- [34] L. Birry, J.H. Zagal, J.P. Dodelet, *Electrochem. Commun.* 12 (2010) 628.
- [35] R.R. Chen, H.X. Li, D. Chu, G.F. Wang, *J. Phys. Chem. C* 113 (2009) 20689.
- [36] S. Chen, W.C. Sheng, N. Yabuuchi, P.J. Ferreira, L.F. Allard, Y. Shao-Horn, *J. Phys. Chem. C* 113 (2009) 1109.
- [37] S.P. Chiao, D.S. Tsai, D.P. Wilkinson, Y.M. Chen, Y.S. Huang, *Int. J. Hydrogen Energy* 35 (2010) 6508.
- [38] A. Ezeta, E.M. Arce, O. Solorza, R.G. Gonzalez, H. Dorantes, J. Alloys Comp. 483 (2009) 429.
- [39] Y.J. Feng, T. He, N. Alonso-Vante, *Electrochim. Acta* 54 (2009) 5252.
- [40] Y.Y. Feng, J.H. Ma, G.R. Zhang, G. Liu, B.Q. Xu, *Electrochem. Commun.* 12 (2010) 1191.
- [41] F. Fouda-Onana, S. Bah, O. Savadogo, *J. Electroanal. Chem.* 636 (2009) 1.
- [42] Y. Garsany, O.A. Baturina, K.E. Swider-Lyons, S.S. Kocha, *Anal. Chem.* 82 (2010) 6321.
- [43] J. Greeley, J.K. Nørskov, *J. Phys. Chem. C* 113 (2009) 4932.
- [44] J.S. Guo, A. Hsu, D. Chu, R.R. Chen, *J. Phys. Chem. C* 114 (2010) 4324.
- [45] S.J. Guo, S.J. Dong, E.K. Wang, *J. Phys. Chem. C* 113 (2009) 5485.
- [46] B.E. Hayden, D. Pletcher, J.P. Suchsland, L.J. Williams, *Phys. Chem. Chem. Phys.* 11 (2009) 9141.
- [47] C.X. He, S.Q. Song, J.C. Liu, V. Maragou, P. Tsiakaras, *J. Power Sources* 195 (2010) 7409.
- [48] J. Hernandez, J. Solla-Gullon, E. Herrero, J.M. Feliu, A. Aldaz, *J. Nanosci. Nanotechnol.* 9 (2009) 2256.
- [49] N. Hoshi, M. Nakamura, S. Kondo, *Electrochem. Commun.* 11 (2009) 2282.
- [50] R.I. Jafri, N. Rajalakshmi, S. Ramaprabhu, *J. Mater. Chem.* 20 (2010) 7114.
- [51] T.Y. Jeon, S.J. Yoo, Y.H. Cho, K.S. Lee, S.H. Kang, Y.E. Sung, *J. Phys. Chem. C* 113 (2009) 19732.
- [52] L. Jiang, A. Hsu, D. Chu, R. Chen, *J. Electrochem. Soc.* 156 (2009) B370.
- [53] S.J. Jiang, Y.W. Ma, G.Q. Jian, H.S. Tao, X.Z. Wang, Y.N. Fan, Y.N. Lu, Z. Hu, Y. Chen, *Adv. Mater.* 21 (2009) 4953.
- [54] J. Kim, Y. Lee, S.H. Sun, *J. Am. Chem. Soc.* 132 (2010) 4996.
- [55] M.H. Lee, J.S. Do, *J. Power Sources* 188 (2009) 353.
- [56] B. Li, J. Prakash, *Electrochem. Commun.* 11 (2009) 1162.
- [57] X.W. Li, J.Y. Liu, W. He, Q.H. Huang, H. Yang, *J. Colloid Interface Sci.* 344 (2010) 132.
- [58] X.W. Li, Y. Zhu, Z.Q. Zou, M.Y. Zhao, Z.L. Li, Q. Zhou, D.L. Akins, H. Yang, *J. Electrochem. Soc.* 156 (2009) B1107.
- [59] C.H. Liang, L. Ding, C.A. Li, M. Pang, D.S. Su, W.Z. Li, Y.M. Wang, *Energy Environ. Sci.* 3 (2010) 1121.
- [60] J.C. Lin, C.L. Chuang, C.M. Lai, H.C. Chu, Y.S. Chen, *Thin Solid Films* 517 (2009) 4728.
- [61] C.W. Liu, Y.C. Wei, K.W. Wang, *J. Colloid Interface Sci.* 336 (2009) 654.
- [62] H. Liu, W. Li, A. Manthiram, *Appl. Catal. B: Environ.* 90 (2009) 184.
- [63] S.H. Liu, C.C. Chiang, M.T. Wu, S.B. Liu, *Int. J. Hydrogen Energy* 35 (2010) 8149.
- [64] Y.W. Ma, H.M. Zhang, H.X. Zhong, T. Xu, H. Jin, X.Y. Geng, *Catal. Commun.* 11 (2010) 434.
- [65] M.R. Miah, M.T. Alam, T. Okajima, T. Ohsaka, *J. Electrochem. Soc.* 156 (2009) B1142.
- [66] K.C. Neyerlin, R. Srivastava, C.F. Yu, P. Strasser, *J. Power Sources* 186 (2009) 261.
- [67] A. Ohma, T. Ichiya, K. Fushinobu, K. Okazaki, *Surf. Sci.* 604 (2010) 965.
- [68] C.V. Rao, B. Viswanathan, *J. Phys. Chem. C* 114 (2010) 8661.
- [69] R. Rego, C. Oliveira, A. Velazquez, P.L. Cabot, *Electrochem. Commun.* 12 (2010) 745.
- [70] C.M. Sanchez-Sanchez, A.J. Bard, *Anal. Chem.* 81 (2009) 8094.
- [71] L. Santos, K.S. Freitas, E.A. Ticianelli, *Electrochim. Acta* 54 (2009) 5246.
- [72] A. Sarkar, A.V. Murugan, A. Manthiram, *J. Mater. Chem.* 19 (2009) 159.
- [73] K. Sasaki, J.X. Wang, H. Naohara, N. Marinkovic, K. More, H. Inada, R.R. Adzic, *Electrochim. Acta* 55 (2010) 2645.
- [74] K. Suarez-Alcantara, O. Solorza-Feria, *J. Power Sources* 192 (2009) 165.
- [75] S. Takenaka, A. Hirata, H. Matsune, M. Kishida, *Chem. Lett.* 39 (2010) 458.
- [76] S. Tominaka, T. Hayashi, Y. Nakamura, T. Osaka, *J. Mater. Chem.* 20 (2010) 7175.
- [77] D. van der Vliet, D.S. Strmcnik, C. Wang, V.R. Stamenkovic, N.M. Markovic, M.T.M. Koper, *J. Electroanal. Chem.* 647 (2010) 29.
- [78] T. Wadayama, N. Todoroki, Y. Yamada, T. Sugawara, K. Miyamoto, Y. Iijima, *Electrochem. Commun.* 12 (2010) 1112.
- [79] C. Wang, H. Daimon, S.H. Sun, *Nano Lett.* 9 (2009) 1493.
- [80] C. Wang, D. van der Vliet, K.C. Chang, H.D. You, D. Strmcnik, J.A. Schlueter, N.M. Markovic, V.R. Stamenkovic, *J. Phys. Chem. C* 113 (2009) 19365.
- [81] G.X. Wang, H.M. Wu, D. Wexler, H.K. Liu, O. Savadogo, *J. Alloys Comp.* 503 (2010) L1.
- [82] B.N. Wanjala, J. Luo, R. Loukrakpam, B. Fang, D. Mott, P.N. Njoki, M. Engelhard, H.R. Naslund, J.K. Wu, L. Wang, O. Malis, C.J. Zhong, *Chem. Mater.* 22 (2010) 4282.
- [83] Y.C. Wei, C.W. Liu, Y.W. Chang, C.M. Lai, P.Y. Lim, L.D. Tsai, K.W. Wang, *Int. J. Hydrogen Energy* 35 (2010) 1864.
- [84] J. Wu, J. Zhang, Z. Peng, S. Yang, F.T. Wagner, H. Yang, *J. Am. Chem. Soc.* 132 (2010) 4984.
- [85] T.H. Yu, Y. Sha, B.V. Merinov, W.A. Goddard, *J. Phys. Chem. C* 114 (2010) 11527.
- [86] J.H. Zeng, S.J. Liao, J.Y. Lee, Z.X. Liang, *Int. J. Hydrogen Energy* 35 (2010) 942.
- [87] H.J. Zhang, Q.Z. Jiang, L.L. Sun, X.X. Yuan, Z.F. Ma, *Electrochim. Acta* 55 (2010) 1107.
- [88] H.J. Zhang, Q.Z. Jiang, L.L. Sun, X.X. Yuan, Z.P. Shao, Z.F. Ma, *Int. J. Hydrogen Energy* 35 (2010) 8295.
- [89] L. Zhang, K. Lee, C.W.B. Bezerra, J.L. Zhang, J.J. Zhang, *Electrochim. Acta* 54 (2009) 6631.
- [90] W. Zhang, R. Wang, H. Wang, Z. Lei, *Fuel Cells* 10 (2010) 734.
- [91] Y. Zhang, Q.H. Huang, Z.Q. Zou, J.F. Yang, W. Vogel, H. Yang, *J. Phys. Chem. C* 114 (2010) 6860.
- [92] J.S. Zheng, X.Z. Wang, J.L. Qiao, D.J. Yang, B. Li, P. Li, H. Iv, J.X. Ma, *Electrochem. Commun.* 12 (2010) 27.
- [93] S. Axnanda, K.D. Cummins, T. He, D.W. Goodman, M.P. Soriaga, *Chem. Phys. Chem.* 11 (2010) 1468.
- [94] Y.G. Ma, P.B. Balbuena, *J. Electrochem. Soc.* 157 (2010) B959.

- [95] F.R. Brushett, H.T. Duong, J.W.D. Ng, R.L. Behrens, A. Wieckowski, P.J.A. Kenis, J. Electrochem. Soc. 157 (2010) B837.
- [96] J. Luo, N. Kariuki, L. Han, L. Wang, C.-J. Zhong, T. He, Electrochim. Acta 51 (2006) 4821.
- [97] B. Fang, J. Luo, P.N. Njoki, R. Loukrakpam, D. Mott, B. Wanjala, X. Hu, C.J. Zhong, Electrochem. Commun. 11 (2009) 1139.
- [98] B. Fang, J. Luo, P.N. Njoki, R. Loukrakpam, B. Wanjala, J. Hong, J. Yin, X. Hu, J. Last, C.J. Zhong, Electrochim. Acta. 55 (2010) 8230.
- [99] T. Jacob, Fuel Cells 6 (2006) 159.
- [100] N.M. Markovic, J.P.N. Ross, Surf. Sci. Rep. 45 (2002) 117.
- [101] Y. Sha, T.H. Yu, Y. Liu, B.V. Merinov, W.A. Goddard, J. Phys. Chem. Lett. 1 (2010) 856.
- [102] H. Imai, M. Matsumoto, T. Miyazaki, S. Fujieda, A. Ishihara, M. Tamura, K. Ota, Appl. Phys. Lett. 96 (2010) 191905.
- [103] L. Wang, G.D. Billing, Chem. Phys. 224 (1997) 65.
- [104] S. Li, L. Zhang, H.S. Liu, M. Pan, L. Zan, J.J. Zhang, Electrochim. Acta 55 (2010) 4403.
- [105] S. Yotsuhashi, Y. Yamada, W.A. Dino, H. Nakanishi, H. Kasai, Phys. Rev. B 72 (2005) 033415.
- [106] P. Gambardella, Z. Slijvancanin, B. Hammer, M. Blanc, K. Kuhnke, K. Kern, Phys. Rev. Lett. 87 (2001) 056103.
- [107] M.P. Hyman, J.W. Medlin, J. Phys. Chem. B 110 (2006) 15338.
- [108] Y.X. Wang, P.B. Balbuena, J. Phys. Chem. B 108 (2004) 4376.
- [109] M.P. Hyman, J.W. Medlin, J. Phys. Chem. B 109 (2005) 6304.
- [110] Z. Slijvancanin, B. Hammer, Surf. Sci. 515 (2002) 235.
- [111] J. Luo, M.M. Maye, V. Petkov, N.N. Kariuki, L. Wang, P. Njoki, D. Mott, Y. Lin, C.J. Zhong, Chem. Mater. 17 (2005) 3086.
- [112] U.A. Paulus, A. Wokaun, G.G. Scherer, T.J. Schmidt, V. Stamenkovic, V. Radmilovic, N.M. Markovic, P.N. Ross, J. Phys. Chem. B 106 (2002) 4181.
- [113] P.B. Balbuena, D. Altomare, L. Agapito, J.M. Seminario, J. Phys. Chem. B 107 (2003) 13671.
- [114] Y. Xu, A.V. Ruban, M. Mavrikakis, J. Am. Chem. Soc. 126 (2004) 4717.
- [115] G. Kresse, J. Hafner, Phys. Rev. B 47 (1993) 558.
- [116] G. Kresse, J. Furthmuller, Phys. Rev. B 54 (1996) 11169.
- [117] G. Kresse, J. Furthmuller, Comput. Mater. Sci. 6 (1996) 15.
- [118] G. Kresse, D. Joubert, Phys. Rev. B 59 (1999) 1758.
- [119] J.P. Perdew, K. Burk, M. Ernzerhof, Phys. Rev. Lett. 77 (1996) 3865.
- [120] L. Xiao, L. Wang, J. Phys. Chem. A 108 (2004) 8605.
- [121] L. Xiao, B. Tollberg, X. Hu, L. Wang, J. Chem. Phys. 124 (2006) 114309.
- [122] W. Zhang, X. Ran, H. Zhao, L. Wang, J. Chem. Phys. 121 (2004) 7717.
- [123] M.M. Sadek, L. Wang, J. Phys. Chem. A 110 (2006) 14036.
- [124] L. Xiao, L. Wang, J. Phys. Chem. B 111 (2007) 1657.
- [125] G. Henkelman, A. Arnaldsson, H. Jónsson, Comput. Mater. Sci. 36 (2006) 354.
- [126] H. Jónsson, Annu. Rev. Phys. Chem. 51 (2000) 623.
- [127] C. Wert, C. Zener, Phys. Rev. 76 (1949) 1169.
- [128] J. Luo, L. Wang, D. Mott, P. Njoki, N. Kariuki, C.J. Zhong, T. He, J. Mater. Chem. 16 (2006) 1665.